Supplementary Information (SI) for Environmental Science: Water Research & Technology.
This journal is © The Royal Society of Chemistry 2025

Supporting Information

UV Photolysis of Peroxynitrite on Micropollutant Degradation: Implications for Oxidative Treatment in Potable Water Reuse

Liang Wu, [†‡] Sitao Liu, [‡] and Haizhou Liu[†‡*]

[†] Environmental Toxicology Program, University of California, Riverside, CA 92521 USA

[‡] Department of Chemical and Environmental Engineering, University of California, Riverside, CA 92521 USA

*Corresponding author, phone: (951) 827-2076; fax: (951) 827-5696

Email: haizhou@engr.ucr.edu

Submitted to *Environmental Science: Water Research & Technology*

(Contributing to an Invited Submission to the 10th anniversary Collection of *ES: WR&T*)

Pages: 31
Figures: 6
Tables: 8

Table of Contents

Text S1. Preparation of peroxynitrite ($ONOO^-$) solutions

A 50-mL mixed solution containing 50 mM sodium nitrite ($NaNO_2$) and 50 mM hydrogen peroxide (H_2O_2) was prepared. Separately, 25 mL each of 1 M hydrochloric acid (HCl) and 1.5 M sodium hydroxide (NaOH) solutions were also prepared. Prior to use, all solutions were chilled in an ice bath for at least 30 minutes.

To synthesize the $ONOO^-$ stock solution, the cold HCl solution was first added to the $NaNO_2/H_2O_2$ mixture, followed immediately by the addition of the cold NaOH solution. Excess H_2O_2 was removed by adding 10 g of manganese dioxide (MnO_2) powder. The mixture was stirred vigorously in an ice bath under continuous nitrogen gas purging for two hours. Afterward, the MnO_2 was removed by filtration through a 0.2-μm membrane filter, yielding the final H_2O_2-free $ONOO^-$ stock solution.

The $ONOO^-$ stock solution (typically 8-12 mM) remains stable for up to 8 hours when stored at pH ≥13. The formation of nitrite (NO_2^-) and nitrate (NO_3^-) as byproducts during synthesis is unavoidable and cannot be removed from the final solution. Based on a nitrogen balance, a representative synthesized stock solution contained a total of 24.81 mM nitrogen species, consisting of approximately 28% $ONOO^-$, 61% NO_2^-, and 11% NO_3^-.[1] The stock $ONOO^-$ solution was standardized per a direct absorbance method at 302 nm.[2]

Text S2. UV photolysis experiments of various photo-oxidants

UV-driven oxidation experiments were conducted using a 50-mL petri dish reactor equipped with continuous magnetic stirring to ensure solution homogeneity. Illumination was provided by a set of five identical low-pressure mercury lamps (254 nm, model UST-300, Ultra Sum Technologies), arranged symmetrically above the reactor to achieve uniform UV irradiance. The photon fluence rate was rigorously quantified using chemical actinometry with atrazine as the actinometric probe. A 50 mL atrazine solution (10 mg L^{-1}) containing 5 mM phosphate buffer (pH 7, controlled) was placed in a 50-mL petri dish reactor equipped with a continuous magnetic stir bar. The reactor was then positioned directly beneath the UV lamps used in this study. At reaction times of 0, 15, 30, 45, 60, 120, 180, 240, and 300 s, 200 μL aliquots were withdrawn and then analyzed. The optical path length of the system was 0.5 cm. According to the literature, the quantum yield and molar absorption coefficient of atrazine at 254 nm are 0.046 mol $Einstein^{-1}$ and 3860 m^2 mol^{-1}, respectively.[3] Using these parameters together with the measured degradation rate of atrazine, as well as Planck's constant (h), the speed of light (c), and Avogadro's constant (N_A), the incident photon flux was calculated according to established literature methods to be 2.84 $mJ \cdot cm^{-2} \cdot s^{-1}$.[4] A target fluence of 850 mJ/cm^2 (photon flux × UV exposure time) was applied in all tests, corresponding to typical UV doses employed in full-scale UV/advanced oxidation process (UV/AOP) systems treating reverse osmosis (RO) permeate in potable water reuse facilities.

To systematically assess the radical-forming potential of conventional photo-oxidants under controlled conditions, all oxidant dosages were fixed at 1.0 mM. These included hydrogen peroxide (H_2O_2), persulfate ($S_2O_8^{2-}$), free chlorine (HOCl), monochloramine (NH_2Cl), and

dichloramine ($NHCl_2$). In all cases, a trace-level concentration (5 μM) of NB was introduced as a selective molecular probe for hydroxyl radical ($HO^{\bullet}$) quantification.[5] This concentration was chosen to maintain low probe reactivity while enabling reliable high performance liquid chromatography coupled with a diode array detector (HPLC-DAD) detection.

To simulate conditions relevant to real-world advanced treatment trains for potable reuse, all experiments were conducted at pH 5.8 using a 60 mM phosphate buffer system, a pH level representative of RO permeate chemistry. Control experiments were conducted to account for direct photolysis of NB, and in each system, the combination of UV light with a single photo-oxidant allowed for isolation and comparison of $HO^{\bullet}$ generation dynamics across different AOP platforms.

Text S3. Determination of $ONOO^-$ decay during UV photolysis

A 3-mL sample was withdrawn from the petri dish UV reactor and then directly transferred to a 3-mL quartz cuvette reactor with a 1 cm path length. The sample absorbance was measured spectrophotometrically at 302 nm, where $ONOO^-$ exhibits a strong absorption band ($\varepsilon = 1670$ M^{-1} cm^{-1}), while NO_2^- ($\varepsilon = 9.136$ M^{-1} cm^{-1}) and NO_3^- ($\varepsilon = 7.0143$ M^{-1} cm^{-1}) absorb negligibly[2], ensuring accurate quantification. The time intervals for the measurement were 0, 1, 5, and 10 min upon UV exposure.

Text S4. Analytical methods for quantitation of oxidants and probe compound

Monochloramine (NH_2Cl) and dichloramine ($NHCl_2$) were measured at 515 nm according to the standard DPD method (expressed as mg/L as Cl_2).[6] Stock solutions of peroxynitrite ($ONOO^-$) were quantified using the direct absorbance method (ε_{302} = 1670 M^{-1} cm^{-1}).[2] The $ONOO^-$ generated from the hydrolytic decay of $NHCl_2$ was quantified using the fluorescence method based on folic acid ($C_{19}H_{19}N_7O_6$).[7] The folic acid working solution contained 1 mM folic acid and 10 mM sodium hydroxide (NaOH). Calibration curves were prepared using 0–5 μM $ONOO^-$ mixed with 15 μM folic acid in borate buffer at pH 10–13. Fluorescence measurements were conducted using a Horiba Aqualog spectrophotometer with an excitation wavelength of 380 nm and an emission wavelength of 460 nm. The sample volume (*i.e.,* dilution factor) was pre-determined through preliminary experiments to ensure that the $ONOO^-$ concentration in the withdrawn samples fell within the calibration range. All colorimetric methods were performed using a VWR spectrophotometer (UV-3100PC UV-VIS).

Immediately after being withdrawn from the petri dish reactor, samples were quenched by the immediate addition of excess sodium thiosulfate. All samples were analyzed within 24 hours of collection. Quantification of NB, 1,4-dioxane, N,N-diethyl-m-toluamide (DEET), carbamazepine, and caffeine was performed using an Agilent 1200 Series high-performance liquid chromatography system equipped with a diode array detector (HPLC-DAD). The mobile phase consisted of 50% ultrapure water and 50% HPLC-grade acetonitrile for NB, DEET, carbamazepine, and caffeine, and 95% ultrapure water with 5% HPLC-grade acetonitrile for 1,4-dioxane. All analyses were conducted at room temperature using an Agilent ZORBAX Eclipse XDB-C18 column (4.6 mm × 150 mm, 5 μm), with a flow rate of 1.0 mL/min and an injection volume of 100 μL under isocratic conditions. The retention times and detection wavelengths

were 1.49 min at 220 nm for caffeine, 2.61 min at 220 nm for carbamazepine, 4.03 min at 220 nm for DEET, 4.48 min at 276 nm for NB, and 2.15 min at 191 nm for 1,4-dioxane.

Concentrations of nitrate (NO_3^-) and nitrite (NO_2^-) were analyzed by ion chromatography (DX-120, Thermo Fisher Scientific) equipped with a conductivity detector. The mobile phase consisted of 4.5 mM sodium carbonate and 1.4 mM sodium bicarbonate. The operating conditions were as follows: Dionex IonPac AS22 anion column (4 × 250 mm), flow rate of 1.2 mL/min, injection volume of 10 μL, and applied current of 31 mA. The retention times of NO_2 and NO_3^- were 5.91 min and 8.08 min, respectively. The measurement was performed at room temperature.

Text S5. Quantification of hydroxyl radicals (HO•) during $ONOO^-$ photolysis experiments

HO• generated during the UV photolysis of $ONOO^-$ was quantified using nitrobenzene (NB) as a probe compound due to its well-characterized reactivity with HO•.[5] The degradation kinetics of NB were monitored to determine steady-state HO• concentrations and cumulative HO• exposures during UV/$ONOO^-$ experiments.

Equation 1 below was utilized for the expression of NB removal:

Equation 1 $$-\frac{d[NB]}{dt} = k_{NB,HO^\bullet}[NB][HO^\bullet]_{ss}$$

Where [NB] is the NB concentration, $[HO^\bullet]_{ss}$ is the steady-state concentration of HO•, and $k_{NB,HO^\bullet}$ (4.7×10^9 $M^{-1}s^{-1}$)[8] is the second-order rate constants of NB reacting with HO•.

To evaluate the UV absorption contribution of each species and its potential to generate HO•, the branching ratio of UV light absorbed was calculated using Equation 2:

Equation 2 $$Branching\ Ratio = \frac{\varepsilon_1 C_1}{\sum \varepsilon_i C_i}$$

Where ε_1 is the molar absorptivity of the specie of interest at 254 nm, and C_1 is the initial concentration of the reactant. Essentially, $\sum \varepsilon_i C_i$ represents the summation of the products of molar absorptivity ε and initial concentrations C for all the reactants present in the UV/$ONOO^-$ system, including NB, $ONOO^-$, NO_2^-, NO_3^-, and OH^-.

Under UV irradiation at 254 nm, NB degradation occurs via multiple pathways: direct photolysis and HO•-mediated oxidation from photolysis of various species in the synthesized $ONOO^-$ solution, including $ONOO^-$, NO_2^-, and NO_3^-.[9] To quantify contributions from each, we define:

D_{obs}: total observed degradation of NB in the UV/$ONOO^-$ system

D_{dir} : contribution from direct photolysis of NB

$D_{NO_2^-}$, $D_{NO_3^-}$, D_{ONOO^-}: contributions from HO• generated via photolysis of NO_2^-, NO_3^-, and $ONOO^-$, respectively

Thus:

Equation 3 $$D_{obs} = \left(D_{dir} + D_{NO_2^-} + D_{NO_3^-} + D_{ONOO^-}\right)$$

To link NB degradation to its corresponding rate constants, we define the degradation fraction D as $D = 1 - C_t/C_0$, where C_0 and C_t are the NB concentrations at time 0 and time t, respectively. Under pseudo-first-order conditions, the degradation of NB over time follows $C_t = C_0 \cdot e^{-k_{obs}t}$, which leads to $D = 1 - e^{-k_{obs}t}$. This relationship allows us to calculate the observed pseudo-first-order degradation rate constant $-k_{obs}$ from experimentally measured NB degradation, providing a basis for separating and quantifying the contributions of individual pathways in the UV/$ONOO^-$ system.

To analyze the contribution of the generated HO• from each species, Equation 4 was used for the description for NB removal when photolyzing $ONOO^-$ solution:

Equation 4 $$Branching\ Ratio = \frac{k_1 C_1}{\sum k_i C_i}$$

Where k_{NB}, k_{ONOO^-}, $k_{NO_2^-}$, and $k_{NO_3^-}$ represent pseudo first-order degradation rates of NB due to UV photolysis of NB, $ONOO^-$, NO_2^-, and NO_3^-, respectively. When photolyzing a 1 mM $ONOO^-$ solution at pH 11, HO• can be generated from multiple sources, including UV/$ONOO^-$, UV/ NO_3^-, and UV/ NO_2^-. Consequently, the UV photolysis of $ONOO^-$, NO_3^-, and NO_2^- can rapidly degrade NB. Additionally, NB exhibits UV absorbance and undergoes rapid direct photolysis. NB (initial

concentration of 5 μM) degradation was quantified and then used to calculate the $HO^{\bullet}$ generation. In the 1 mM $ONOO^-$ solution at pH 11, the molar absorptivity of each species is provided in Figure S1, and the branching ratios are calculated as follows:

Table S1. Branching ratios of UV light absorbed during UV photolysis of $ONOO^-$ at pH 11.

Component	Absorptivity ε_{254nm} ($M^{-1}cm^{-1}$)	Initial Conc'n (mM)	Branching Ratio
$ONOO^-$	347	1	85.67%
NB	5983	0.005	7.39%
NO_2^-	12.3	2.17	6.59%
NO_3^-	3.63	0.374	0.34%
OH^-	0.1	1	0.01%

To calculate the generated $HO^{\bullet}$ from $ONOO^-$ photolysis only, a series of control experiments were conducted. Since OH^- does not contribute to $HO^{\bullet}$ generation when photolyzed, the first control experiment was the direct photolysis of NB at neutral pH of 7.

Table S2. Branching ratios of UV light absorbed during the direct photolysis of NB at pH 7.

Component	Absorptivity ε_{254nm} ($M^{-1}cm^{-1}$)	Initial Conc'n (mM)	Branching Ratio
NB	5983	0.005	100.00%
OH^-	0.1	0.0001	0.00%

Since the NB absorbs 100% of the UV light at pH 7, the degradation of NB was determined, and k_{NB}, the direct photolysis rate for NB, was calculated according to Equation 1. The second control experiment was the direct photolysis of NB at pH 11.

Table S3. Branching ratios of UV light absorbed during the direct photolysis of NB at pH 11.

Component	Absorptivity ε_{254nm} ($M^{-1}cm^{-1}$)	Initial Conc'n (mM)	Branching Ratio
NB	5983	0.005	99.67%
OH^-	0.1	1	0.33%

The percentage of UV light absorbed by NB was altered when the solution pH increased from 7 to 11. Therefore, the adjusted NB degradation (defined as $k_{NB}^{adjusted}$) was calculated from k_{NB} since the branching ratio was calculated ($k_{NB}^{adjusted} = k_{NB} \times branching\ ratio$) in Table S2. In addition, k_{OH^-} was calculated. The third control experiment was the UV photolysis of NB with 2.17 mM NO_2^- at pH 11.

Table S4. Branching ratios of UV light absorbed during UV photolysis of NB with 2.17 mM NO_2^- at pH 11.

Component	Absorptivity ε_{254nm} ($M^{-1}cm^{-1}$)	Initial Conc'n (mM)	Branching Ratio
NB	5983	0.005	52.75%
NO_2^-	12.3	2.17	47.07%
OH^-	0.1	1	0.18%

$k_{NB}^{adjusted}$ and $k_{OH^-}^{adjusted}$ ($k_{OH^-}^{adjusted} = k_{OH^-} \times branching\ ratio$) were calculated according to Table S4. Then, using the same approach, $k_{NO_2^-}$ was calculated. The fourth control experiment was the UV photolysis of NB with 0.374 mM NO_3^- at pH 11.

Table S5. Branching ratios during UV photolysis of NB with 0.374 mM NO_3^- at pH 11.

Component	Absorptivity ε_{254nm} ($M^{-1}cm^{-1}$)	Initial Conc'n (mM)	Branching Ratio
NB	5983	0.005	95.47%
NO_3^-	3.63	0.374	4.21%
OH^-	0.1	1	0.32%

$k_{NB}^{adjusted}$ and $k_{OH^-}^{adjusted}$ were calculated according to Table S5, and $k_{NO_3^-}$ was also calculated. All the degradation rates of NB were calculated, and the overall NB degradation was determined in the UV photolysis of 1 mM $ONOO^-$, the NB degradation due to UV/$ONOO^-$, which is, D_{ONOO^-}, was calculated according to Equations 3 and 4. Therefore, $HO^\bullet$ generation was calculated.

Cumulative exposure of NB to HO• over time was used to evaluate the oxidative capacity of the UV/ONOO$^-$ system. According to the method by Elovitz and Gunten, cumulative HO• exposure was calculated according to Equation 5.[10]

Equation 5 $$\ln\left\{\frac{C}{C_0}\right\} = -k_{NB,HO\bullet}\int [HO^\bullet]dt$$

C_0 represents the initial NB concentration, which is 5 μM before UV exposure, C is the NB concentration at a UV exposure time t, $k_{NB,HO\bullet}$ (4.7×10^9 M^{-1}s^{-1})[8] is the second-order rate constant between HO• and NB, and $\int [HO^\bullet]dt$ represents the cumulative HO• exposure of NB. To show $\int [HO^\bullet]dt$ more straightforwardly, Equation 4 is rearranged to the below equation (Equation 6).

Equation 6 $$\int [HO^\bullet]dt = \frac{\ln\left\{\frac{C}{C_0}\right\}}{-k_{NB,HO\bullet}}$$

The degradation of NB due to UV photolysis of ONOO$^-$, which is k_{ONOO^-}, can be used to calculate the cumulative HO• exposure by Equation 6.

The same approach was used to quantify HO• generated in the UV/ONOO$^-$ system for other model micropollutants, including 1,4-dioxane, N,N-diethyl-m-toluamide (DEET), caffeine, and carbamazepine. For calculating the HO•-induced degradation of each micropollutant, reaction rate constants were selected based on values widely cited in the literature. Specifically, rate constants of 3.1×10^9 M^{-1}s^{-1} for 1,4-dioxane and 4.7×10^9 M^{-1}s^{-1} for nitrobenzene (NB) were adopted directly due to their consistent reporting. For DEET, caffeine, and carbamazepine, where reported values vary significantly, the average of the literature-reported rate constants was used: 6.3×10^9 M^{-1}s^{-1} for DEET, 6.7×10^9 M^{-1}s^{-1} for caffeine, and 6.7×10^9 M^{-1}s^{-1} for carbamazepine. A summary of the selected HO• reaction rate constants for the five model micropollutants is provided below in Table S6.[8,11–19]

Table S6. Summary of the rate constants of micropollutants with HO•.

Micropollutants	$k_{HO•}$ ($\times 10^9$ $M^{-1}s^{-1}$)	References
1,4-dioxane	2.4–3.1	*10, 11*
NB	3.2–4.7	*7, 12*
DEET	5.0–7.5	*13, 15, 16*
caffeine	6.4-6.9	*13, 14*
carbamazepine	4.6–8.8	*17, 18*

Text S6. Intrinsic quantum yield model of HO• in the UV/ONOO- system

Equation 7 $$k_{\mathrm{obs}} = 2.303\Phi_{\mathrm{obs}} I_0 \varepsilon + k_{\cdot HO,ONOO^-}[HO\cdot]_{ss}$$

Where Φ_{obs} represents the concentration-dependent quantum yield of $ONOO^-$ under UV photolysis at 254 nm, k_{obs} is the experimentally determined overall decay rate of $ONOO^-$ (s^{-1}), I_0 is the incident photon flux (Ein cm^{-2} s^{-1}) determined by atrazine actinometry, ε is the molar absorption coefficient of $ONOO^-$ at 254 nm (347 M^{-1} cm^{-1}), and $[HO\cdot]_{ss}$ is the steady-state concentration of HO•. The factor 2.303 is used to convert from base-10 to natural logarithm in accordance with the Beer–Lambert law. Since the HO• generated by UV photolysis of $ONOO^-$ reacts rapidly with $ONOO^-$ itself (4.8×10^9 M^{-1} s^{-1}), Equation 7 was used to calculate the intrinsic concentration-dependent Φ_{obs}. The decay of both NB and $ONOO^-$ were experimentally determined in the UV/$ONOO^-$ system across a range of initial $ONOO^-$ concentrations. This enabled determination of a series of Φ_{obs} values from an extensive dataset covering $ONOO^-$ concentrations from 0.05 to 5 mM.

Equation 8 $$\Phi = \frac{\Phi_{obs}\cdot(K+[\mathrm{ONOO^-}]\cdot \mathrm{BR})}{[\mathrm{ONOO^-}]\cdot \mathrm{BR}}$$

Where Φ denotes the quantum yield achieved when the majority of generated HO• is available to react with target micropollutants (*i.e.,* under negligible self-scavenging conditions), Φ_{obs} represents the concentration-dependent quantum yield of $ONOO^-$ under UV photolysis at 254 nm. [$ONOO^-$] is the initial $ONOO^-$ (M), and BR is the branching ratio representing the fraction of HO• that reacts with $ONOO^-$ (Equation 4). The parameter K (M) is the half-saturation constant, defined as the value of [$ONOO^-$] × BR at which the observed quantum yield reaches half of its maximum (Φ_{obs} = Φ/2). To determine Φ, a series of Φ_{obs} values were derived using Equation 7 across a broad range of initial $ONOO^-$ concentrations (0.05 to 5 mM). The quantum

yield from this dataset was assigned as Φ. Nonlinear regression of Equation 8 to the experimental data yielded best-fit values of $\Phi = 0.452$ mol Ein^{-1} and $K = 1.28 \times 10^{-4}$ M, with an $R^2 = 0.976$. These results indicate that $ONOO^-$ self-scavenging significantly limits $HO^\bullet$ availability at elevated $ONOO^-$ concentrations, and the model provides a robust framework for predicting effective radical exposure as a function of $ONOO^-$ concentration and solution conditions.

With $k_{HO\cdot,NB} = 4.7\times10^9$ M^{-1} s^{-1} and [NB] = 5 μM used as the $HO^\bullet$ probe, once Φ_{obs} was calculated from the concentration-dependent model, the corresponding steady-state $HO^\bullet$ concentration was determined using the following expression:

Equation 9 $$[HO\cdot]_{ss} = \frac{2.303\cdot\varepsilon\cdot\Phi_{obs}\cdot I_0}{k_{HO\cdot,NB}\cdot[NB]+k_{HO\cdot,ONOO^-}\cdot[ONOO^-]}$$

This formulation links the rate of $HO^\bullet$ generation from $ONOO^-$ photolysis to its scavenging by $ONOO^-$ and NB, providing a mechanistic estimate of $[HO\cdot]_{ss}$ as a function of $ONOO^-$ concentration and solution matrix. The model enables estimation of $HO^\bullet$ steady-state levels in UV/$ONOO^-$ systems based on $ONOO^-$ levels and known optical parameters, allowing direct comparison with other UV-based advanced oxidation processes (UV/AOPs).

Text S7. Estimation of $ONOO^-$ Concentration in Realistic RO Permeate and $HO^\bullet$ Generation Potential

To evaluate the *in situ* oxidative capacity of the UV/$ONOO^-$ system in a realistic aerated reverse osmosis (RO) permeate matrix, we estimated the steady-state $ONOO^-$ concentration formed via $NHCl_2$ (3 mg/L as Cl_2) hydrolysis and used it to calculate the resulting $HO^\bullet$ generation via the quantum yield model described in Text S6.

Estimation of [$ONOO^-$] from $NHCl_2$ Hydrolysis:

Based on our prior study[20], in a realistic aerated RO permeate matrix with pH adjusted to the optimal value of 8.4 for non-UV oxidative capacity, the $ONOO^-$ concentration was estimated using the following steps:

1. The pseudo-first-order degradation rate of 1,4-dioxane (1,4-D) under non-UV $NHCl_2$ hydrolysis conditions at $TOTCO_3$ = 0.2 mM was extracted from Figure 5B of our previous work, yielding $k_{1,4-\text{dioxane}}$ = 0.015 s^{-1}.

2. Using the second-order rate constant for the reaction between 1,4-D and $HO^\bullet$ (k = 3.1×10^9 M^{-1} s^{-1}), the steady-state $HO^\bullet$ concentration was back-calculated:

$$[\text{HO}\cdot]_{\text{ss}} = \frac{k_{1,4-\text{dioxane}}}{k_{1,4-\text{dioxane,HO}\cdot}} = \frac{0.015}{3.1\times10^{9}} = 4.84\times10^{-12}\text{M}$$

3. Given a branching ratio of 9.43% for $HO^\bullet$ reacting with 1,4-D at 0.2 mM $TOTCO_3$ (interpolated from Table S5 of our prior study[20]), the total $HO^\bullet$ concentration before scavenging was estimated as:

$$[\text{HO}\cdot]\ \text{total} = \frac{[\text{HO}\cdot]\text{ss}}{0.0943} = \frac{4.84\times10^{-12}}{0.0943} = 5.13\times10^{-10}\text{M}$$

4. The conversion fraction of $ONOO^-$ to ONOOH at pH 8.4 was evaluated based on the following reaction pathways:

(1) $ONOO^- + CO_2$: $k = 2.9\times10^4\ M^{-1}\ s^{-1}$

$$k_{\text{eff}} = k_{\text{CO2}} \cdot [\text{CO}_2] = 2.9 \times 10^4 \times 2.0 \times 10^{-4} = 5.8\ \text{s}^{-1}$$

(2) $ONOO^- \leftrightarrow$ ONOOH ($pK_a = 6.6$), ONOOH decay rate $k = 0.35\ s^{-1}$

$$f_{\text{ONOOH}} = \frac{[\text{ONOOH}]}{[\text{ONOOH}] + [ONOO^-]} = \frac{0.0158}{1 + 0.0158} = 0.01556$$

According to literature, ONOOH leads to homolysis to $HO^\bullet$ and NO_3^-, and 28% of ONOOH decays lead to $HO^\bullet$.[21] Thus, ONOO- ↔ ONOOH → $HO^\bullet$:

$$k_{\text{ONOOH}} = f_{\text{ONOOH}} \times 0.28 \times\ 0.35 = 0.01556 \times 0.28 \times 0.35 = 0.001524\ \text{s}^{-1}$$

(3) $ONOO^- \rightarrow NO_3^-$: $k = 9.6\times10^{-6}\ s^{-1}$

(4) $ONOO^- \rightarrow NO^\bullet$ and $O_2^{\bullet-}$: $k = 2.0\times10^{-2}\ s^{-1}$

$$k_{\text{total}}\ = 5.8 + 0.001524 + 9.6 \times 10^{-6} + 2.0 \times 10^{-2} \approx 5.8215\ \text{s}^{-1}$$

Resulting in a calculated $ONOO^-$ ↔ ONOOH branching ratio of 0.02617%.

6. From this, the bulk $ONOO^-$ concentration was estimated:

$$[\text{ONOO}^-] = \frac{[\text{ONOOH}]}{0.0002617} = 1.96 \times 10^{-7}\text{M}$$

Application to the UV/$ONOO^-$ Model:

Using this $ONOO^-$ concentration, the $HO^\bullet$ + $ONOO^-$ branching ratio was recalculated as:

$$\mathrm{BR} = \frac{k_{\mathrm{HO}\cdot,ONOO^-} \cdot [\mathrm{ONOO^-}]}{k_{\mathrm{HO}\cdot,\mathrm{NB}}[\mathrm{NB}] + k_{\mathrm{HO}\cdot,ONOO^-} \cdot [\mathrm{ONOO^-}]} = 3.85\%$$

Plugging into the quantum yield model:

$$\Phi_{obs} = \frac{0.452 \times (1.96 \times 10^{-7}) \cdot 0.0385}{1.28 \times 10^{-4} + (1.96 \times 10^{-7}) \cdot 0.0385} = 2.66 \times 10^{-5}$$

The steady-state HO• concentration generated under UV irradiation was then calculated as:

$$[\mathrm{HO}\cdot]_{\mathrm{ss}} = \frac{2.303 \times 347 \times 2.66 \times 10^{-5} \times 3 \times 10^{-6}}{4.7 \times 10^{9} \times 5 \times 10^{-6} + 4.8 \times 10^{9} \times 1.96 \times 10^{-7}} = 2.61 \times 10^{-12}\ \mathrm{M}$$

The direct photolysis rate of $ONOO^-$ at 254 nm was calculated as:

$$-\frac{dC}{dt} = \Phi k_{\mathrm{a,254nm}}$$

where Φ is the quantum yield of $ONOO^-$ ($mol \cdot Einstein^{-1}$); k_a,254nm is the specific rate of 254-nm light absorption by $ONOO^-$. The latter is given by:

$$k_{\mathrm{a,254nm}} = \mathrm{I}_{\mathrm{UV,254nm}} \mathrm{F}_s \mathrm{F}_{\mathrm{p}}$$

Here, F_s is the fraction of 254-nm photons absorbed by the system, and F_p is the fraction of photons absorbed specifically by $ONOO^-$, expressed as:

$$\mathrm{F}_s = 1 - 10^{-\left(\sum_{i=1}^{i} \varepsilon_i c_i\right)1}, \mathrm{F}_{\mathrm{p}} = \frac{\varepsilon_{\mathrm{PFAS}} \mathrm{C}_{\mathrm{PFAS}}}{\sum_{i=1}^{i} \varepsilon_i c_i}$$

where ε_i and C_i are the molar absorption coefficients and concentrations, respectively, of all light-absorbing constituents. Relevant absorptivities at 254 nm include: (0.1 $M^{-1}\ cm^{-1}$), $ONOO^-$ OH^- (347 $M^{-1}\ cm^{-1}$), NO_3^- ($\varepsilon_{NO_3^-,254\ nm}$= 3.63 $M^{-1}\ cm^{-1}$), NO_2^- (12.3 $M^{-1}\ cm^{-1}$), and NB

(5983 M^{-1} cm^{-1}); *l* is the effective light pathlength. Given the strong UV absorbance of these species, the term $F_s \approx 1$, indicating complete photon absorption by the system.

Substituting these terms yields the direct photolysis rate constant for $ONOO^-$:

$$k_{254nm}\ (s^{-1}) = \frac{I_{UV,254nm}\varepsilon_{ONOO^-}\Phi_{ONOO^-}}{\sum_{i=1}^{n}\varepsilon_i c_i}$$

The incident 254-nm photon flux $I_{UV,254nm}$ was measured by atrazine actinometry as 3.0×10^{-6} Einstein $L^{-1}s^{-1}$. Under these conditions, the direct photolysis rate of $ONOO^-$ ranged from 3.12×10^{-7} to 1.31×10^{-6} s^{-1}, substantially greater than the intrinsic decay rate of ONOOH (k = 0.35 s^{-1}). Thus, during 254-nm irradiation, $HO^{\bullet}$ generation arises additively from both $ONOO^-$ protonation and $ONOO^-$ photolysis, as the rapid protonation of $ONOO^-$ to ONOOH proceeds concurrently with its slower photolysis, ensuring that both pathways contribute to overall radical formation.

In summary, under realistic RO permeate conditions with pH adjusted to 8.4, the estimated steady-state $HO^{\bullet}$ in fresh and aerated matrices are 3.22×10^{-12} M and 4.83×10^{-12} M, respectively. Based on $ONOO^-$ decay kinetics from our previous study, leveraging the residual $ONOO^-$ in RO permeate by introducing UV irradiation can enhance the oxidative capacity by 54% to 81%, depending on the aeration level (Figure S6). This highlights the potential for UV/$ONOO^-$ as a supplementary AOP to augment $NHCl_2$ hydrolysis in water reuse applications.

Text S8. Branching ratio calculation of HO• in the UV/ONOO⁻ system

The HO• generated from UV photolysis of $ONOO^-$ reacts concurrently with both NB and $ONOO^-$, with second-order rate constants of 4.7×10^9 $M^{-1}s^{-1}$ and 4.8×10^9 $M^{-1}s^{-1}$, respectively.[8,22]

Using Equation 4, the branching ratios of HO• reacting with NB and $ONOO^-$ were calculated and are presented in Table S7 below.

Table S7. Branching ratios of HO• reactions with NB and $ONOO^-$ at an initial $ONOO^-$ concentration of 0.05 mM.

Component	Rate Constant with HO• ($M^{-1}s^{-1}$)	Initial Concentration (mM)	Branching Ratio with HO•	Reference
NB	4.7×10^9	0.005	8.92%	*7*
$ONOO^-$	4.8×10^9	0.05	91.08%	*21*

The same approach was applied to calculate branching ratios under varying initial $ONOO^-$ concentrations during UV/$ONOO^-$ experiments. The results are presented in Table S8 below.

Table S8. Branching ratios of HO• reactions with NB and $ONOO^-$ at initial $ONOO^-$ concentrations ranging from 0.1 to 5 mM.

Component	$ONOO^-$ 0.1 mM	$ONOO^-$ 0.25 mM	$ONOO^-$ 0.5 mM	$ONOO^-$ 1 mM	$ONOO^-$ 2 mM	$ONOO^-$ 3 mM	$ONOO^-$ 4 mM	$ONOO^-$ 5 mM
NB	4.67%	1.92%	0.97%	0.49%	0.24%	0.16%	0.12%	0.1%
$ONOO^-$	95.33%	98.08%	99.03%	99.51%	99.76%	99.84%	99.88%	99.9%

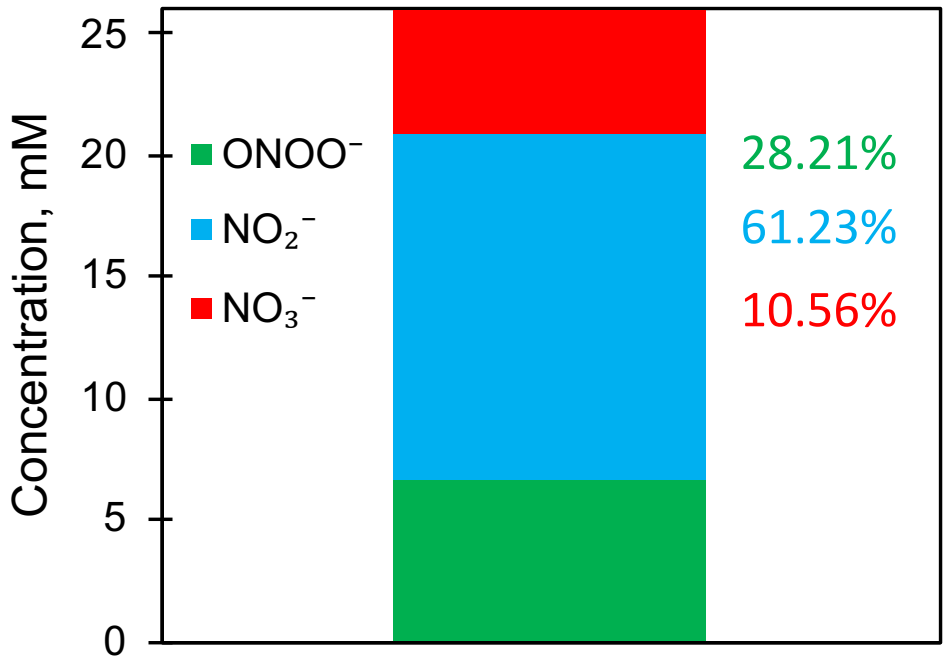

Figure S1. Composition of the synthesized stock $ONOO^-$. Composition of 1 mM synthesized $ONOO^-$: $[ONOO^-]_0$ = 1 mM, $[NO_2^-]_0$ = 2.17 mM, $[NO_3^-]_0$ = 0.374 mM, $[OH^-]_0$ = 100 mM, pH = 13.

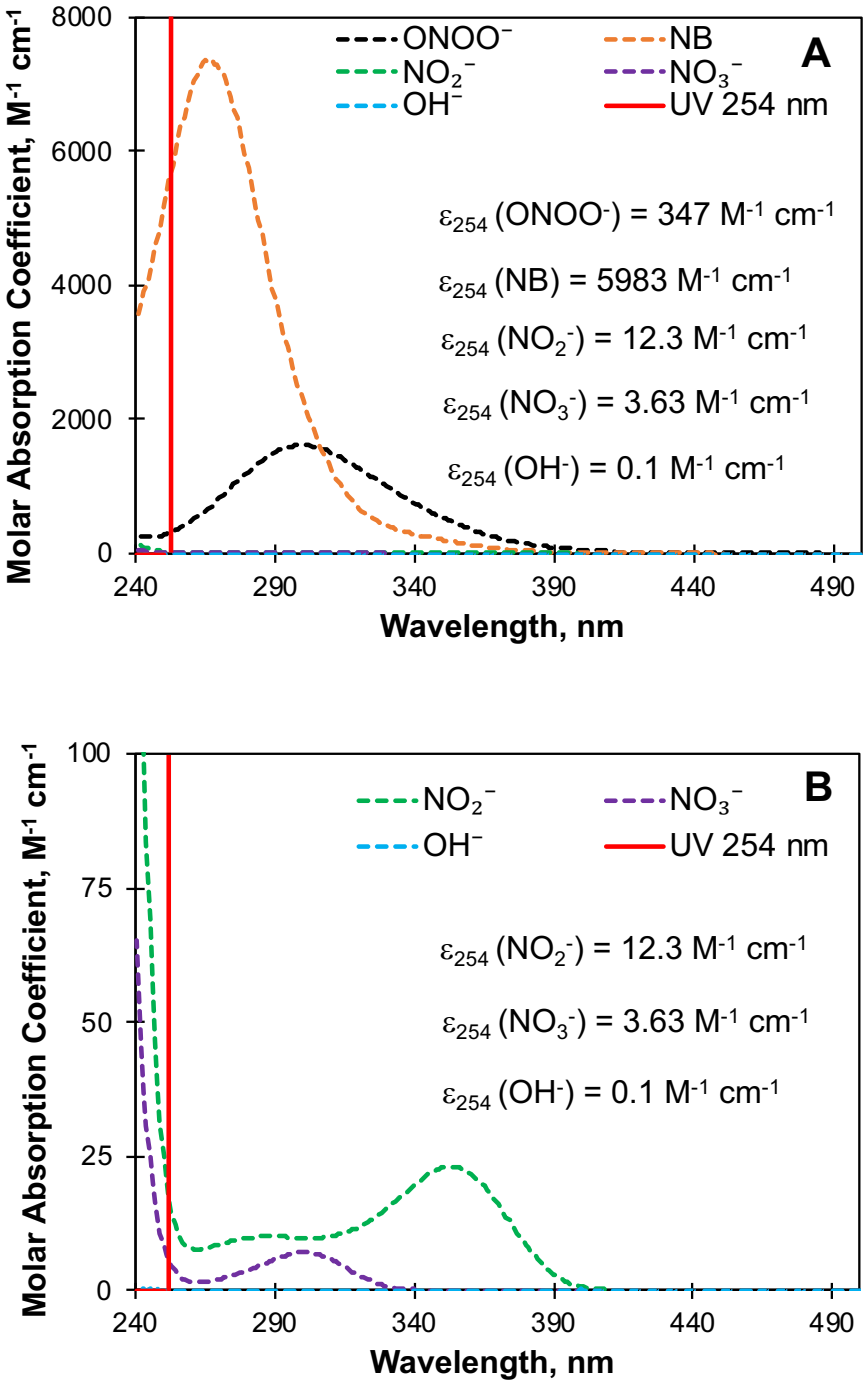

Figure S2. Molar absorption coefficient. (A) $ONOO^-$, NB, NO_2^-, NO_3^-, and OH^-; (B) NO_2^-, NO_3^-, and OH^-.

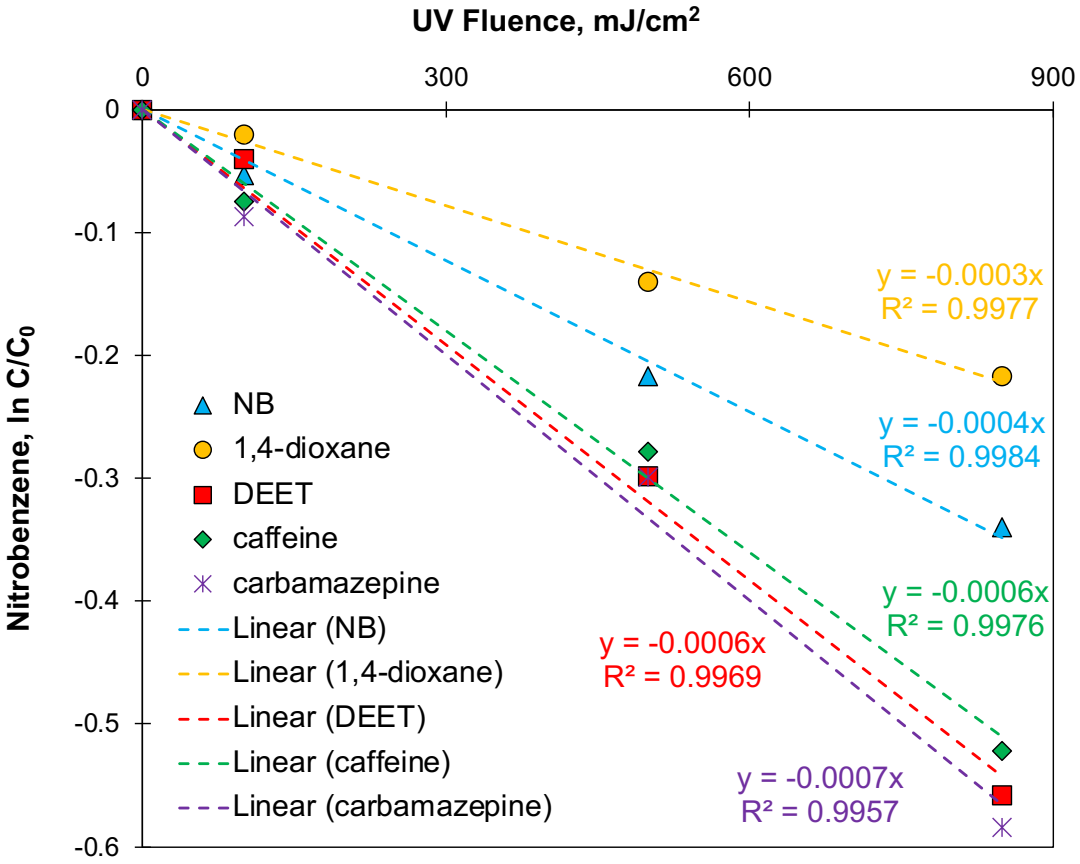

Figure S3. Normalized degradation rates of five model micropollutants due to UV/$ONOO^-$ at pH 11. $[NB]_0$ = 5 µM, $[1,4\text{-dioxane}]_0$ = 5 µM, $[DEET]_0$ = 5 µM, $[caffeine]_0$ = 5 µM, $[carbamazepine]_0$ = 5 µM, [NaOH] = 1 mM, $[ONOO^-]_0$ = 1 mM, $[NO_2^-]_0$ = 2.17 mM, $[NO_3^-]_0$ = 0.374 mM, UV Fluence = 0, 100, 500 and 850 mJ/cm^2.

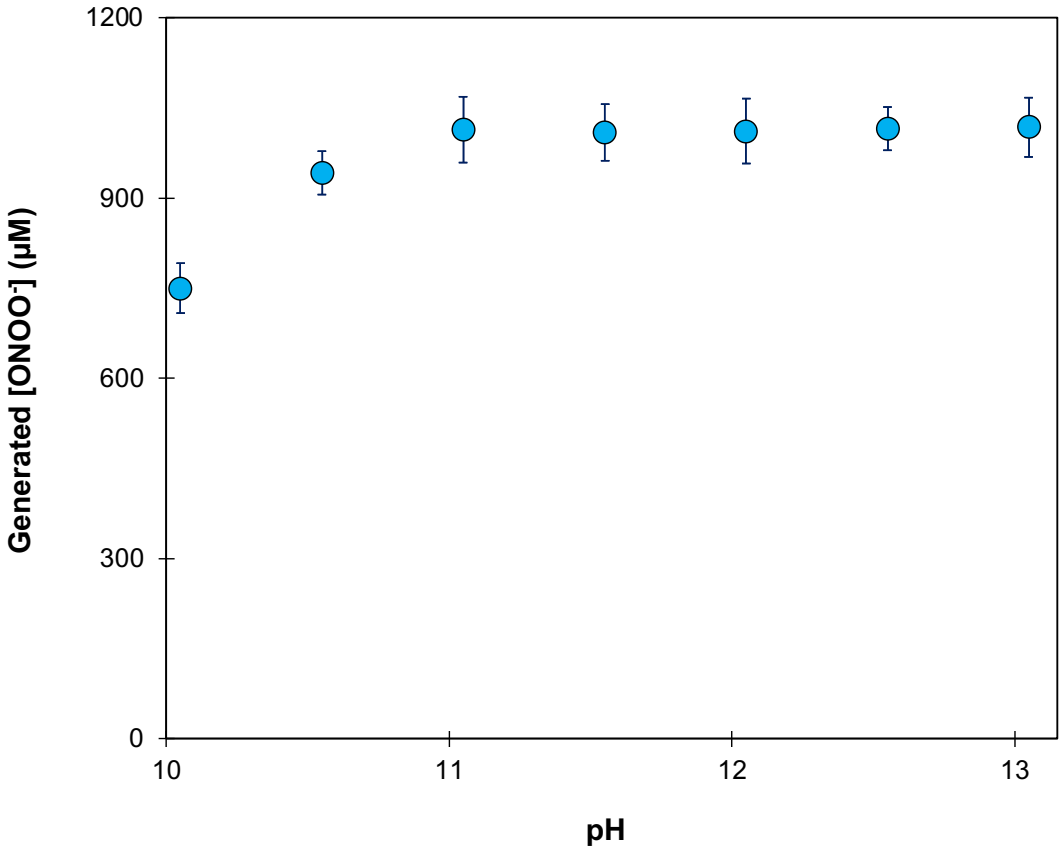

Figure S4. $ONOO^-$ formation via $NHCl_2$ hydrolysis at pH 10-13. Borate buffer = 60 mM, $[NHCl_2]_0$ = 3 mM, hydrolysis time = 15 s, folic acid = 15 μM in the diluted solution.

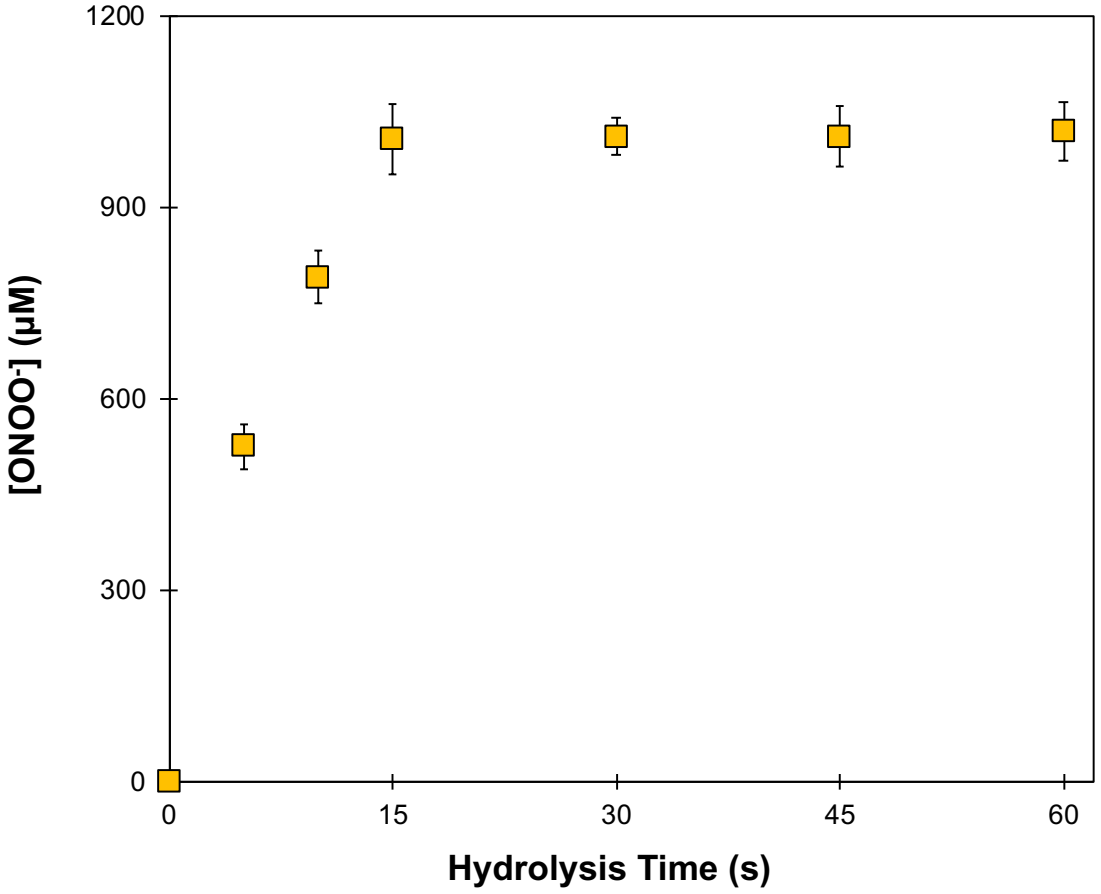

Figure S5. $ONOO^-$ generation via $NHCl_2$ hydrolysis at pH 11. Borate buffer = 60 mM, $[NHCl_2]_0$ = 3 mM, folic acid = 15 μM in the diluted solution.

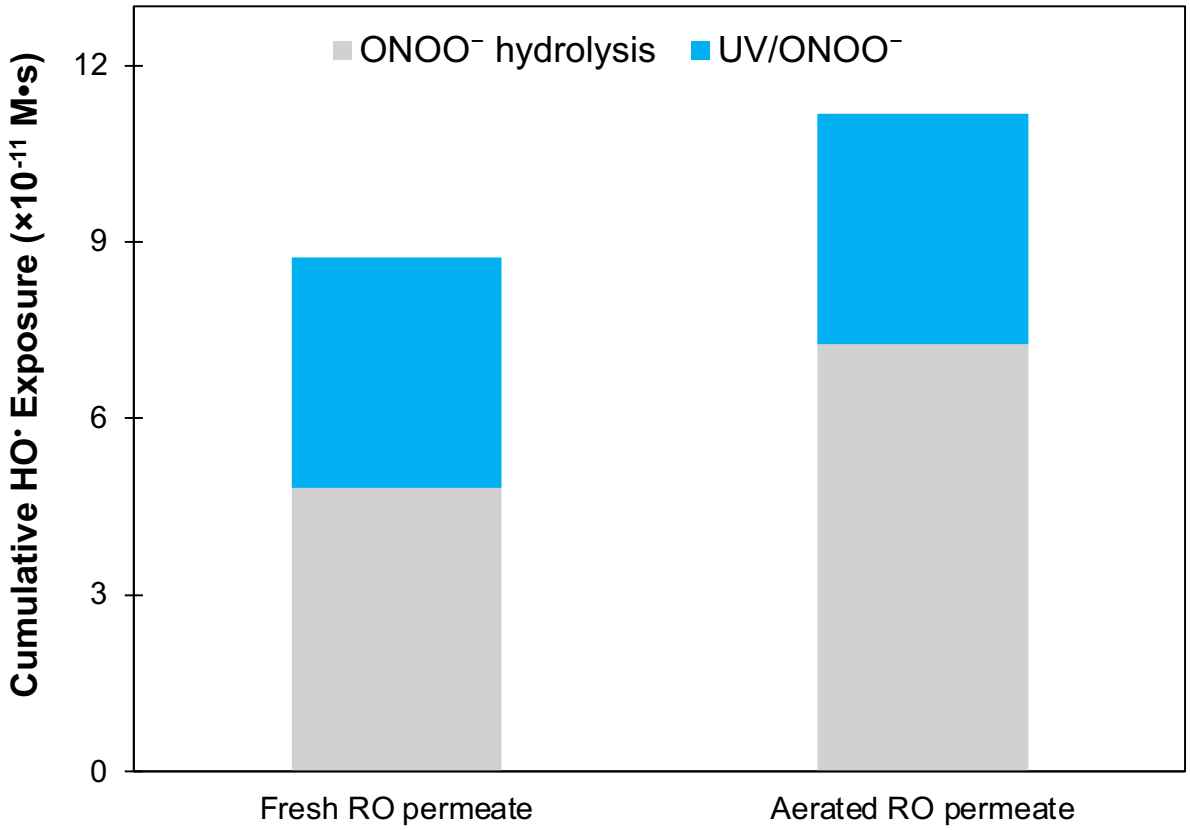

Figure S6. Predicted cumulative HO• exposure contribution from the non-UV pathway of $NHCl_2$ hydrolysis compared with the UV photolysis of $ONOO^-$ under realistic RO permeate conditions. All predictions are based on the assumption that the RO permeate pH is raised from 5.2 to 8.4. Fresh RO permeate: $[TOTCO_3]_0$ = 1.6 mM; aerated RO permeate: $[TOTCO_3]_0$ = 0.2 mM; $[NHCl_2]_0$ = 3 mg/L, $[NH_2Cl]_0$ = 2.1 mg/L, $[NB]_0$ = 0.8 μM, reaction time = 15 s. The cumulative HO• exposure contribution from UV/$ONOO^-$ is estimated using the mathematical model (details of the calculations are provided in Text S7).

References

(1) Pfeiffer, S.; Gorren, A. C. F.; Schmidt, K.; Werner, E. R.; Hansert, B.; Bohle, D. S.; Mayer, B. Metabolic Fate of Peroxynitrite in Aqueous Solution. Reaction with Nitric Oxide and PH-Dependent Decomposition to Nitrite and Oxygen in a 2:1 Stoichiometry. *J. Biol. Chem.* **1997**, *272* (6), 3465–3470.

(2) Hughes, M. N.; Nicklin, H. G. The Chemistry of Pernitrites. Part I. Kinetics of Decomposition of Pernitrous Acid. *J. Chem. Soc. A Inorganic, Phys. Theor.* **1968**, No. 450, 450–452.

(3) Hessler, D. P.; Gorenflo, V.; Frimmel, F. H. Degradation of Aqueous Atrazine and Metazachlor Solutions by UV and UV/ H2O2-Influence of PH and Herbicide Concentration. *Acta Hydrochim. Hydrobiol.* **1993**, *21* (4), 209–214.

(4) Canonica, S.; Meunier, L.; von Gunten, U. Phototransformation of Selected Pharmaceuticals during UV Treatment of Drinking Water. *Water Res.* **2008**, *42* (1–2), 121–128.

(5) Watts, M. J.; Linden, K. G. Chlorine Photolysis and Subsequent OH Radical Production during UV Treatment of Chlorinated Water. *Water Res.* **2007**, *41* (13), 2871–2878.

(6) Clesceri, L. S.; Greenberg, S. E.; Trussell, R. R. *Standard Methods for the Examination of Water and Wastewater*, 17th ed.; American Public Health Association: Washington DC, 1989.

(7) Huang, J. C.; Li, D. J.; Diao, J. C.; Hou, J.; Yuan, J. L.; Zou, G. L. A Novel Fluorescent Method for Determination of Peroxynitrite Using Folic Acid as a Probe. *Talanta* **2007**, *72* (4), 1283–1287.

(8) Asmus, K. D.; Cercek, B.; Ebert, M.; Henglein, A.; Wigger, A. Pulse Radiolysis of Nitrobenzene Solutions. *Trans. Faraday Soc.* **1967**, *63* (5), 2435–2441.

(9) Li, Y.; Wang, L.; Xu, H.; Lu, J.; Chovelon, J. M.; Ji, Y. Direct and Nitrite-Sensitized Indirect Photolysis of Effluent-Derived Phenolic Contaminants under UV254irradiation. *Environ. Sci. Process. Impacts* **2022**, *24* (1), 127–139.

(10) Elovitz, M. S.; Von Gunten, U. Hydroxyl Radical/Ozone Ratios during Ozonation Processes. I. The R(Ct) Concept. *Ozone Sci. Eng.* **1999**, *21* (3), 239–260.

(11) Thomas, J. K. Rates of Reaction of the Hydroxyl Radical. *Trans. Faraday Soc.* **1965**, *61*, 702–707.

(12) Eibenberger, J. Pulse Radiolytic Investigations Concerning the Formation and the Oxidation of Organic Radicals in Aqueous Solutions, Vienna University, 1980.

(13) NETA, P.; DORFMAN, L. M. Pulse Radiolysis Studies. XIII. Rate Constants for the Reaction of Hydroxyl Radicals with Aromatic Compounds in Aqueous Solutions. **1968**, No. 18, 222–230.

(14) Sun, P.; Lee, W. N.; Zhang, R.; Huang, C. H. Degradation of DEET and Caffeine under UV/Chlorine and Simulated Sunlight/Chlorine Conditions. *Environ. Sci. Technol.* **2016**, *50* (24), 13265–13273.

(15) Kesavan, P. C.; Powers, E. L. Differential Modification of Oxic and Anoxic Components of Radiation Damage in Bacillus Megaterium Spores by Caffeine. *Int. J. Radiat. Biol.* **1985**, *48* (2), 223–233.

(16) Javier Benitez, F.; Acero, J. L.; Real, F. J.; Roldan, G.; Rodriguez, E. Modeling the Photodegradation of Emerging Contaminants in Waters by UV Radiation and UV/H2O2 System. *J. Environ. Sci. Heal. - Part A Toxic/Hazardous Subst. Environ. Eng.* **2013**, *48* (1), 120–128.

(17) Song, W.; Cooper, W. J.; Peake, B. M.; Mezyk, S. P.; Nickelsen, M. G.; O'Shea, K. E. Free-Radical-Induced Oxidative and Reductive Degradation of N,N′-Diethyl-m-Toluamide (DEET): Kinetic Studies and Degradation Pathway. *Water Res.* **2009**, *43* (3), 635–642.

(18) Xiao, R.; Ma, J.; Luo, Z.; Zeng, W.; Wei, Z.; Spinney, R.; Hu, W. P.; Dionysiou, D. D. Experimental and Theoretical Insight into Hydroxyl and Sulfate Radicals-Mediated Degradation of Carbamazepine. *Environ. Pollut.* **2020**, *257*, 113498.

(19) Ali, F.; Khan, J. A.; Shah, N. S.; Sayed, M.; Khan, H. M. Carbamazepine Degradation by UV and UV-Assisted AOPs: Kinetics, Mechanism and Toxicity Investigations. *Process Saf. Environ. Prot.* **2018**, *117*, 307–314.

(20) Wu, L.; Liu, S.; Liu, H. Dichloramine Hydrolysis in Membrane Desalination Permeate: Mechanistic Insights and Implications for Oxidative Capacity in Potable Reuse Applications. *Environ. Sci. Technol.* **2024**, *58* (29), 13157–13167.

(21) Goldstein, S.; Rabani, J. Mechanism of Nitrite Formation by Nitrate Photolysis in Aqueous Solutions: The Role of Peroxynitrite, Nitrogen Dioxide, and Hydroxyl Radical. *J. Am. Chem. Soc.* **2007**, *129* (34), 10597–10601.

(22) Goldstein, S.; Saha, A.; Lymar, S. V.; Czapski, G. Oxidation of Peroxynitrite by Inorganic Radicals: A Pulse Radiolysis Study. *J. Am. Chem. Soc.* **1998**, *120* (22), 5549–5554.